Supplementary Materials

Biological metal–organic frameworks for natural gas purification and MTO product separation

Wen Li[1], Dan Wang[1], Yi Wang[2], Zhaohui Shi[1], Junxue Liu[1], Lirong Zhang[1], Dongxu Xue[2], Yunling Liu[1,*]

[1]State Key Laboratory of Inorganic Synthesis and Preparative Chemistry, College of Chemistry, Jilin University, Changchun 130012, Jilin, China.
[2]Key Laboratory of Applied Surface and Colloid Chemistry, Ministry of Education, Xi'an Key Laboratory of Organometallic Material Chemistry, School of Chemistry & Chemical Engineering, Shaanxi Normal University, Xi'an 710062, Shaanxi, China.

*Correspondence to: Prof. Yunling Liu, State Key Laboratory of Inorganic Synthesis and Preparative Chemistry, College of Chemistry, Jilin University, 2699 Qianjin Street, Changchun 130012, Jilin, China. E-mail: yunling@jlu.edu.cn
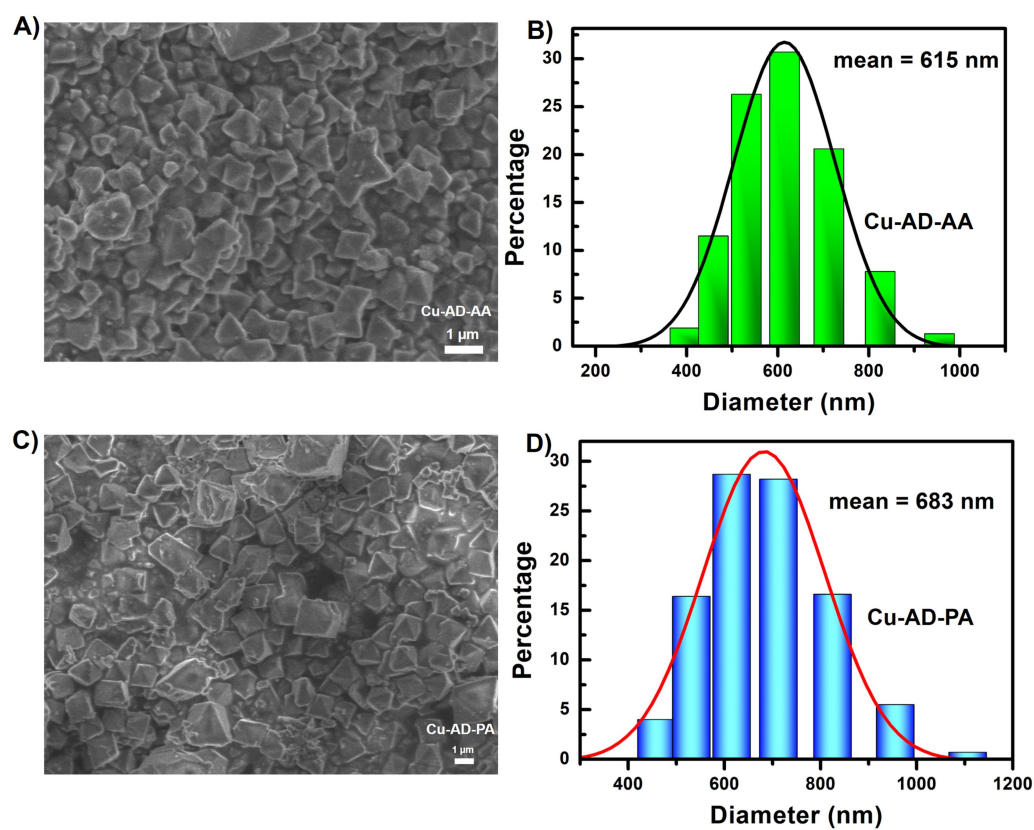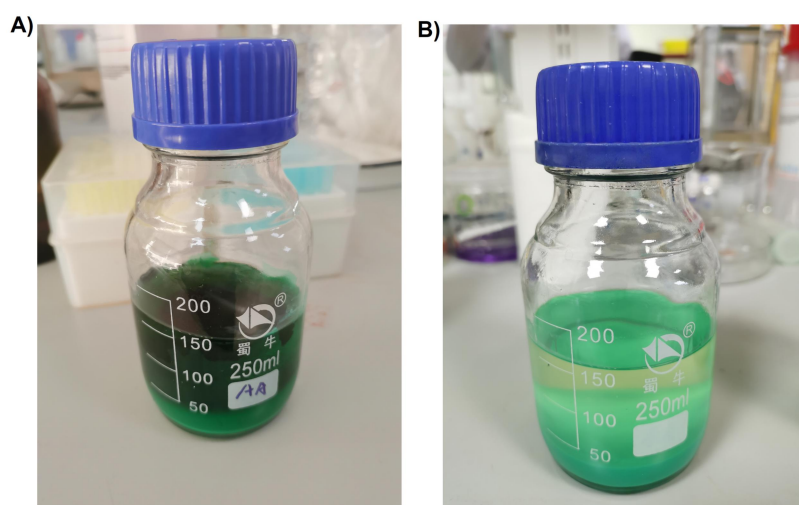
Supplementary Figure 1. SEM images for (A) **Cu-AD-AA**, (C) **Cu-AD-PA** and particle size distributions for (B) **Cu-AD-AA**, (D) **Cu-AD-PA**.

Supplementary Figure 2. Photo of 250 mL glass reaction bottle for (A) **Cu-AD-AA**, (B) **Cu-AD-PA** after the synthesis.
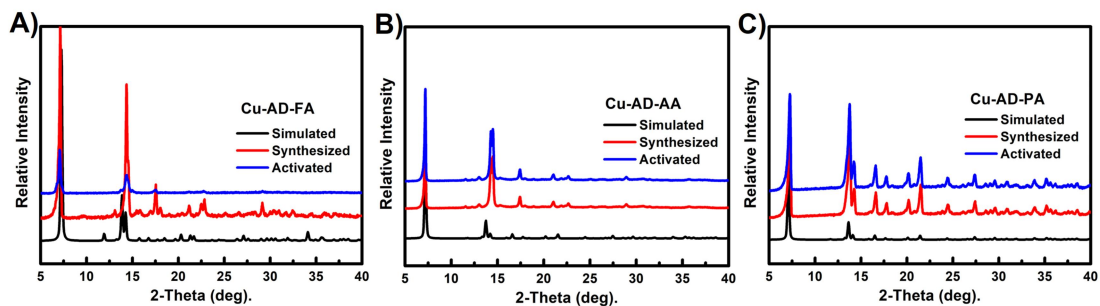
Supplementary Figure 3. PXRD patterns of the simulated, as-synthesized and activated for (A) **Cu-AD-FA**, (B) **Cu-AD-AA** and (C) **Cu-AD-PA**.
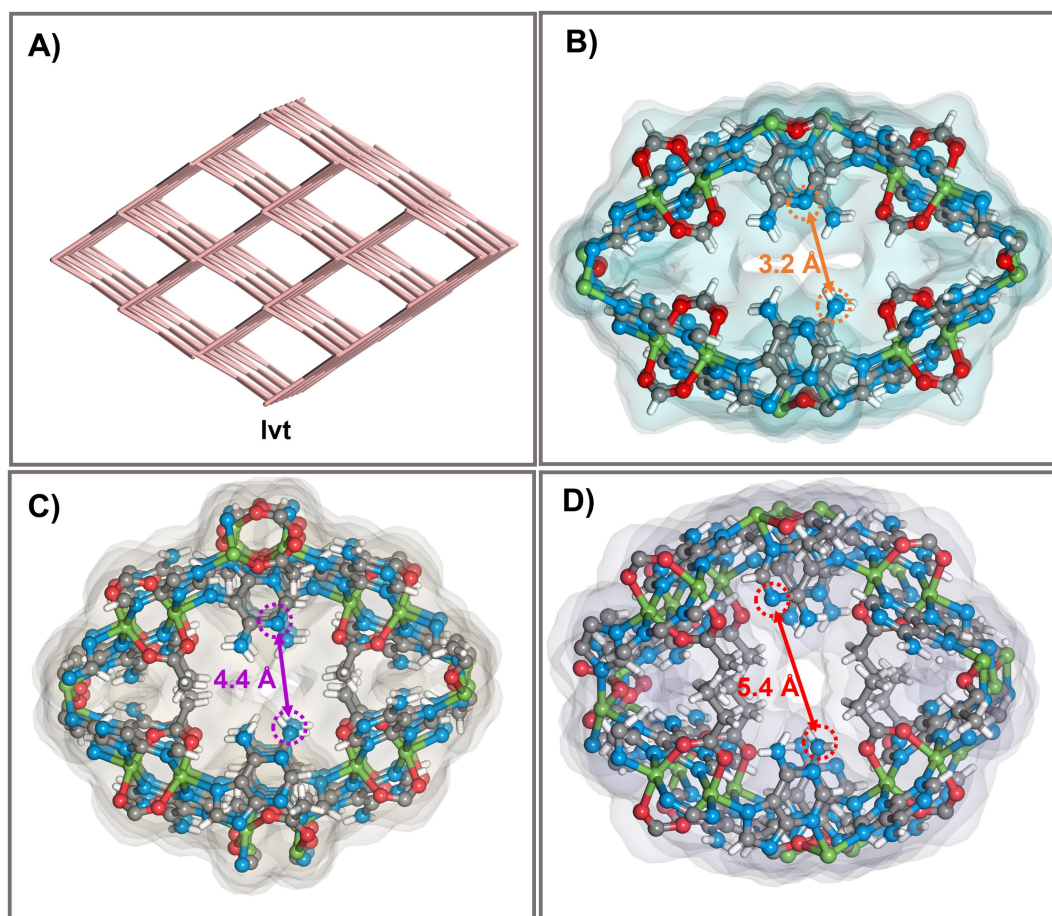

Supplementary Figure 4. (A) Topology view for **lvt** net; (B) Ball-stick view with connolly background for one pore in **Cu-AD-FA**; (C) Ball-stick view with connolly background for one pore in **Cu-AD-AA**; (D) Ball-stick view with connolly background for one pore in **Cu-AD-PA**.
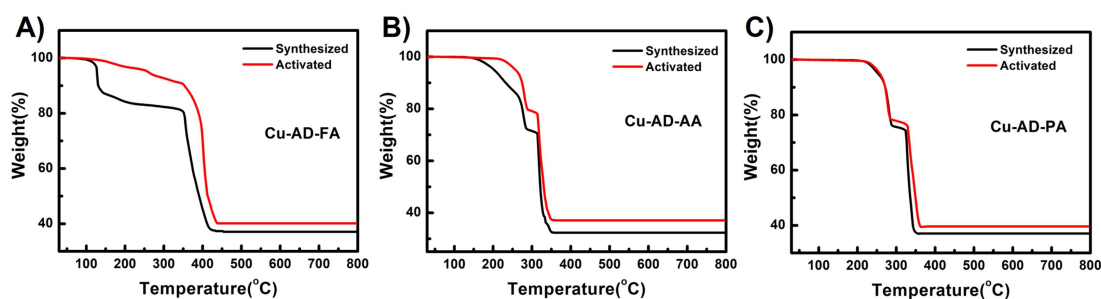
Supplementary Figure 5. TGA curves of the as-synthesized and activated samples for (A) **Cu-AD-FA**, (B) **Cu-AD-AA** and (C) **Cu-AD-PA**.
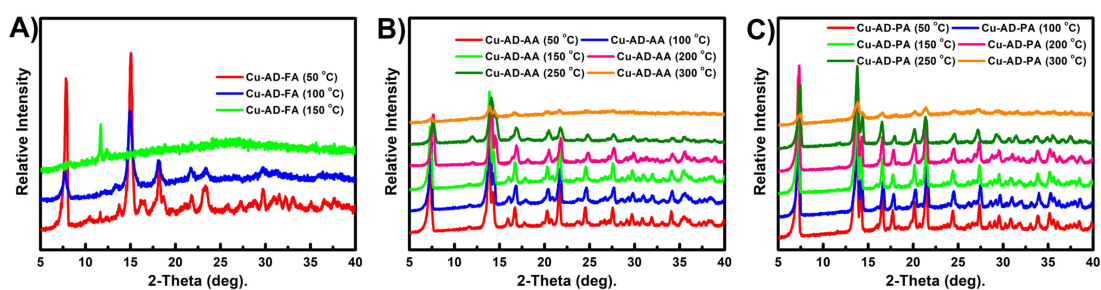
Supplementary Figure 6. PXRD patterns for (A) **Cu-AD-FA**, (B) **Cu-AD-AA** and (C) **Cu-AD-PA** with different temperature treatment.
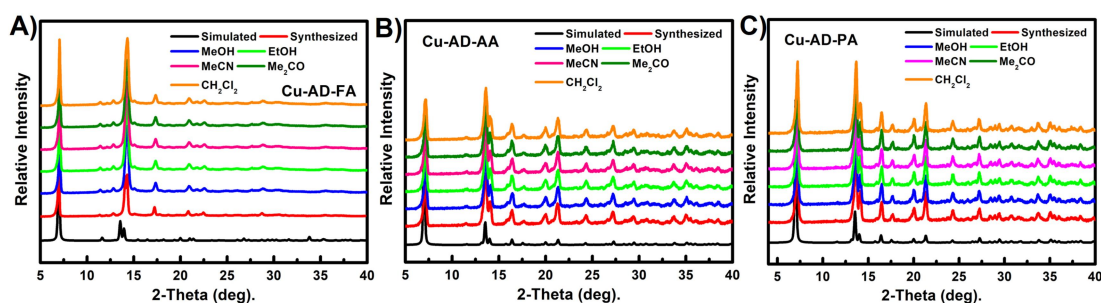
Supplementary Figure 7. PXRD patterns for (A) **Cu-AD-FA**, (B) **Cu-AD-AA** and (C) **Cu-AD-PA** samples after immersed in different organic solvents for 3 days at room temperature.
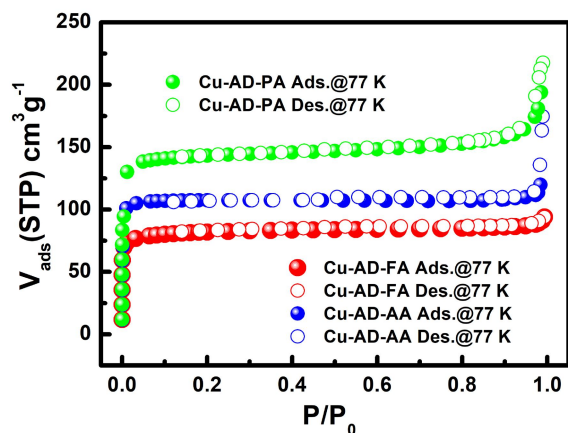
Supplementary Figure 8. N_2 adsorption-desorption isotherms for **Cu-AD-FA**, **Cu-AD-FA** and **Cu-AD-PA** samples after water immersion.
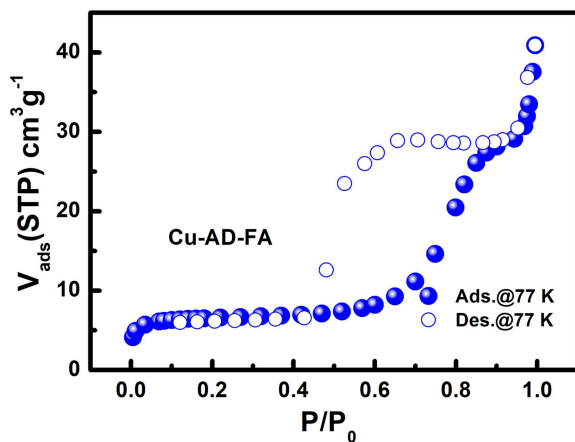
Supplementary Figure 9. N_2 adsorption-desorption isotherm for **Cu-AD-FA** after 90 °C pretreatment.
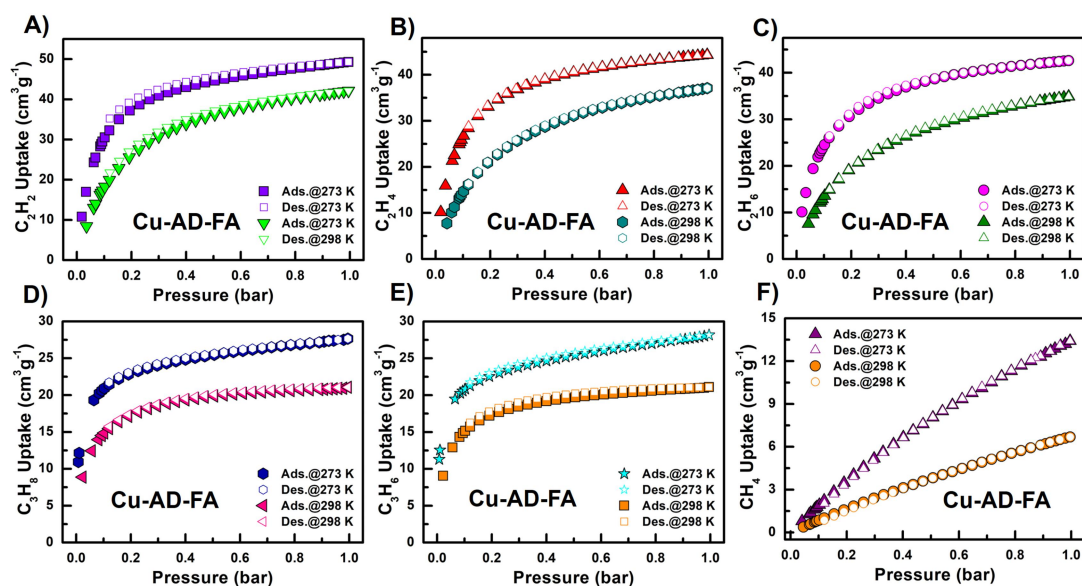
Supplementary Figure 10. (A) C_2H_2, (B) C_2H_4, (C) C_2H_6, (D) C_3H_8, (E) C_3H_6 and (F) CH_4 adsorption-desorption isotherms for **Cu-AD-FA**.
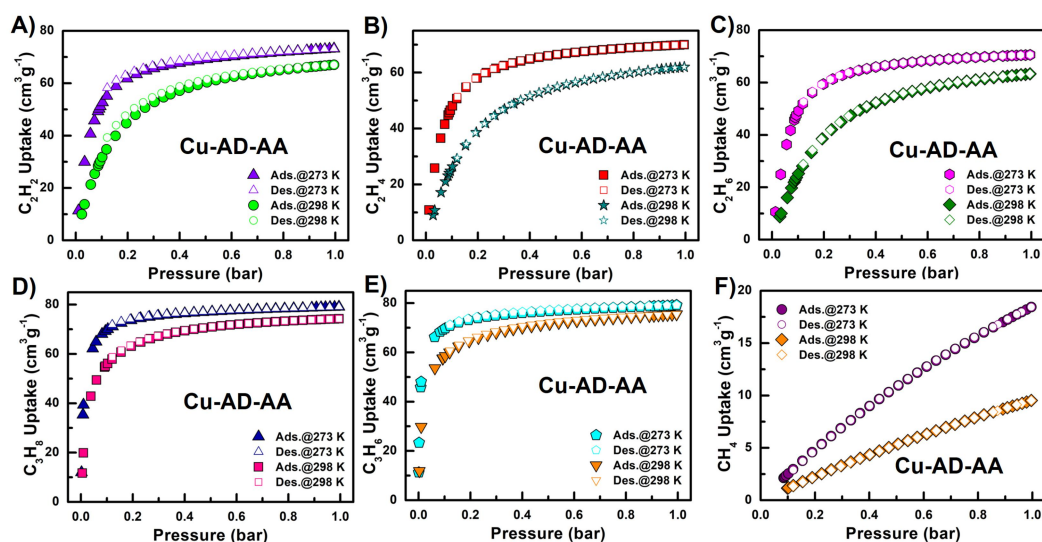
Supplementary Figure 11. (A) C_2H_2, (B) C_2H_4, (C) C_2H_6, (D) C_3H_8, (E) C_3H_6 and (F) CH_4 adsorption-desorption isotherms for **Cu-AD-AA**.
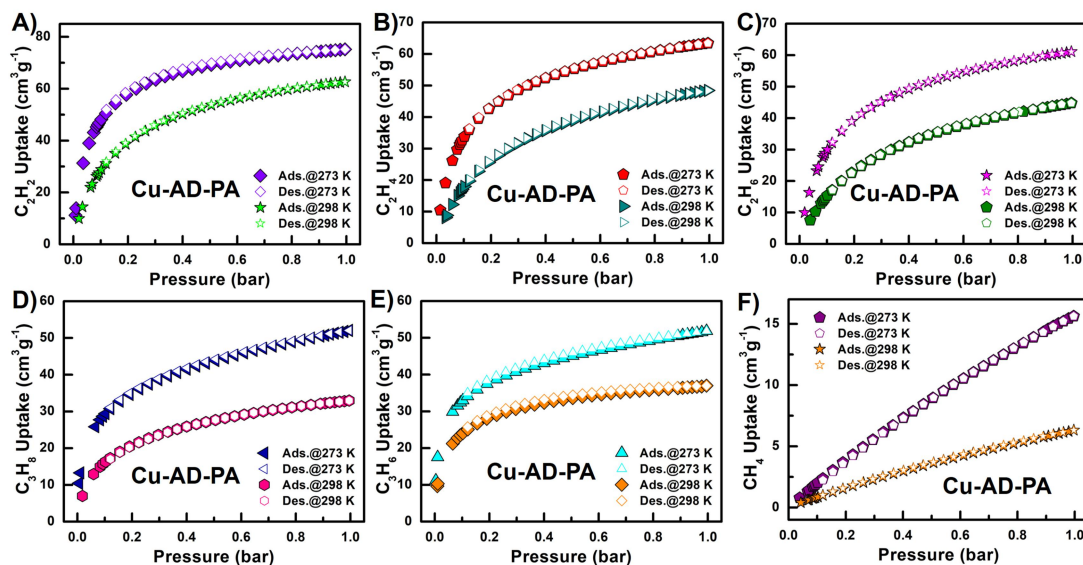
Supplementary Figure 12. (A) C_2H_2, (B) C_2H_4, (C) C_2H_6, (D) C_3H_8, (E) C_3H_6 and (F) CH_4 adsorption-desorption isotherms for **Cu-AD-PA**.
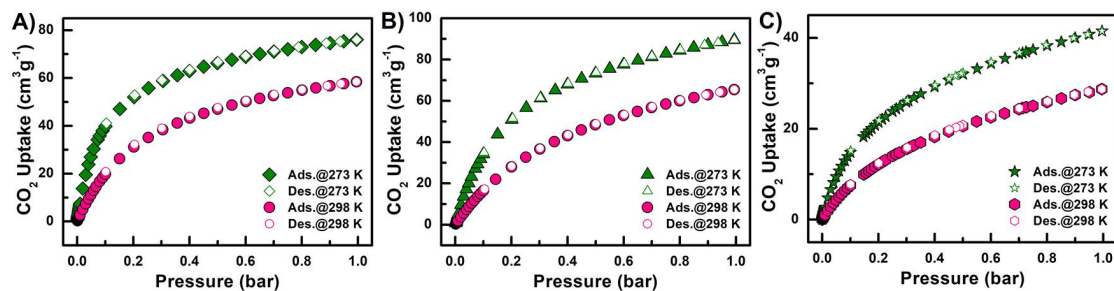
Supplementary Figure 13. CO_2 adsorption-desorption isotherms for (A) **Cu-AD-FA**, (B) **Cu-AD-AA**, (C) **Cu-AD-PA**.
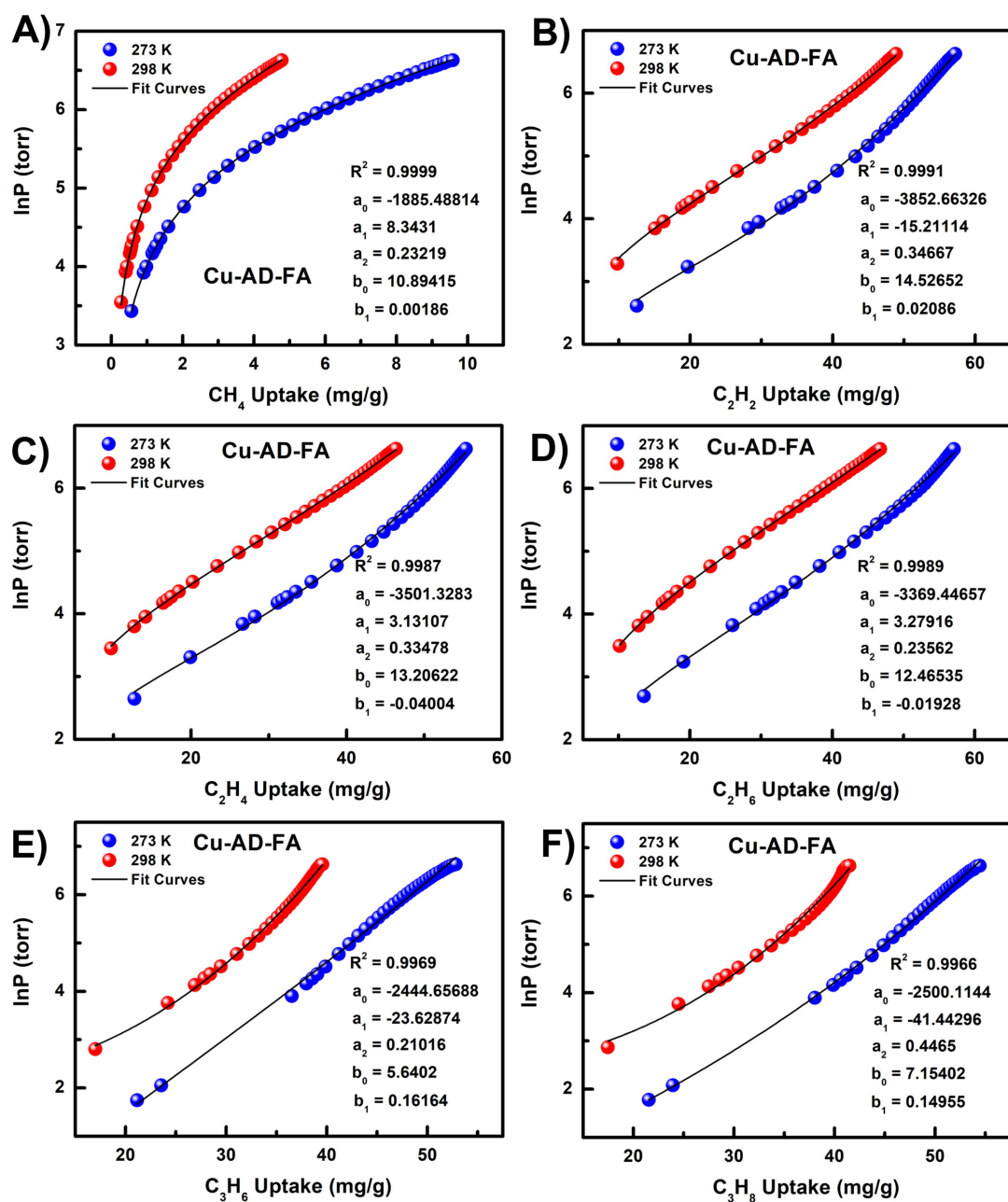
Supplementary Figure 14. Nonlinear curves fitting of (A) CH_4, (B) C_2H_2, (C) C_2H_4, (D) C_2H_6, (E) C_3H_6, and (F) C_3H_8 for **Cu-AD-FA**.
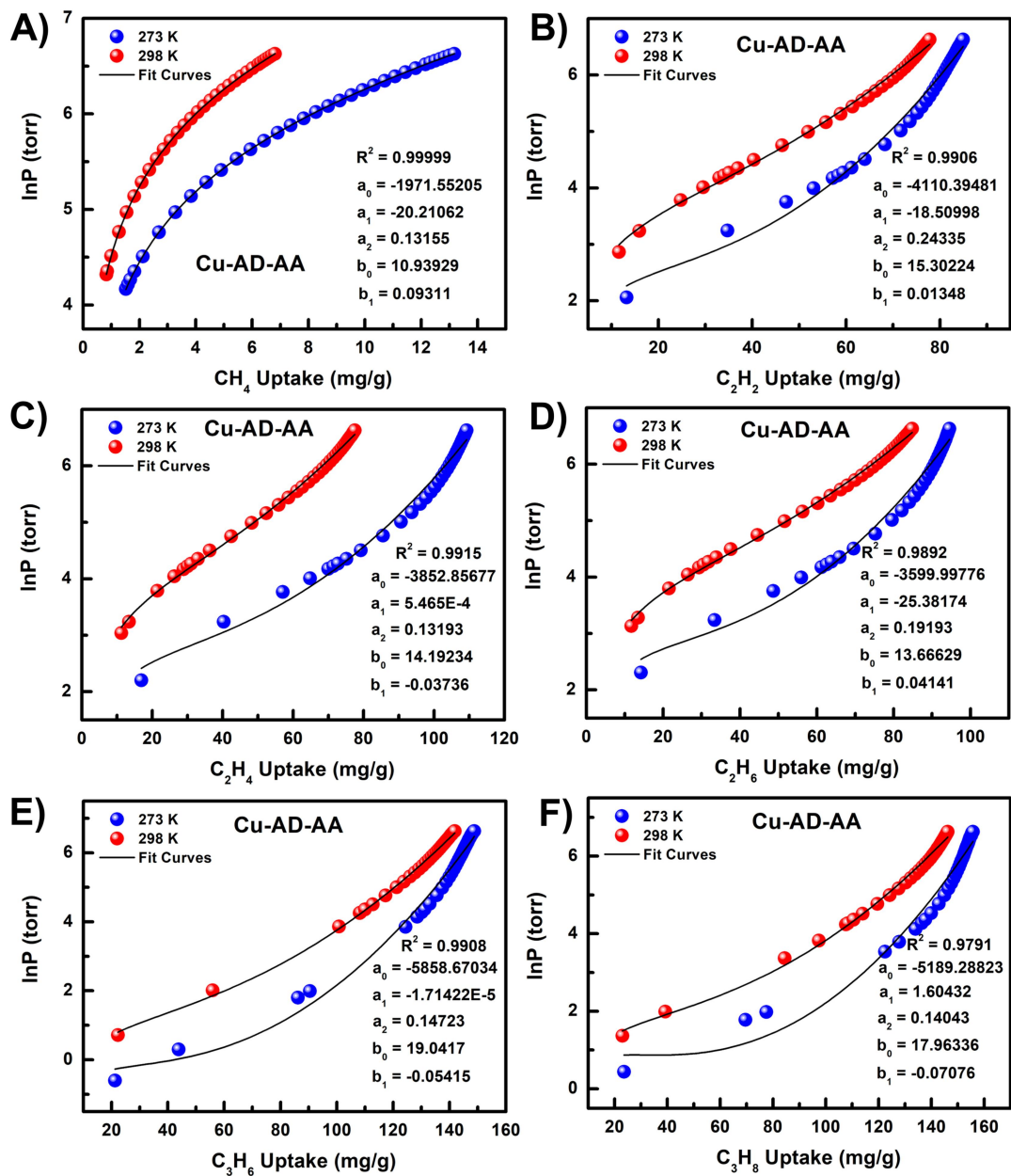
Supplementary Figure 15. Nonlinear curves fitting of (A) CH_4, (B) C_2H_2, (C) C_2H_4, (D) C_2H_6, (E) C_3H_6, and (F) C_3H_8 for **Cu-AD-AA**.
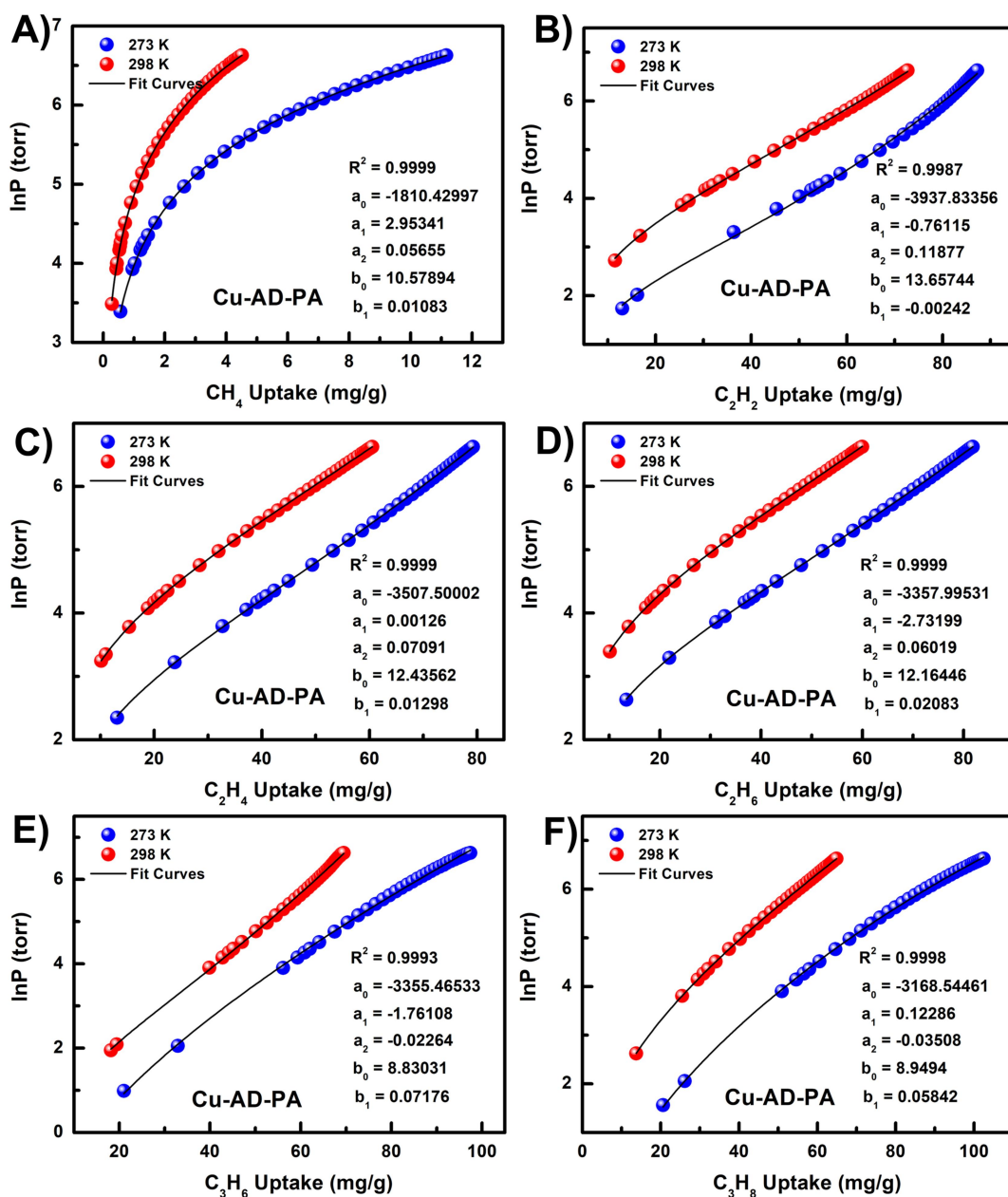
Supplementary Figure 16. Nonlinear curves fitting of (A) CH_4, (B) C_2H_2, (C) C_2H_4, (D) C_2H_6, (E) C_3H_6, and (F) C_3H_8 for **Cu-AD-PA**.
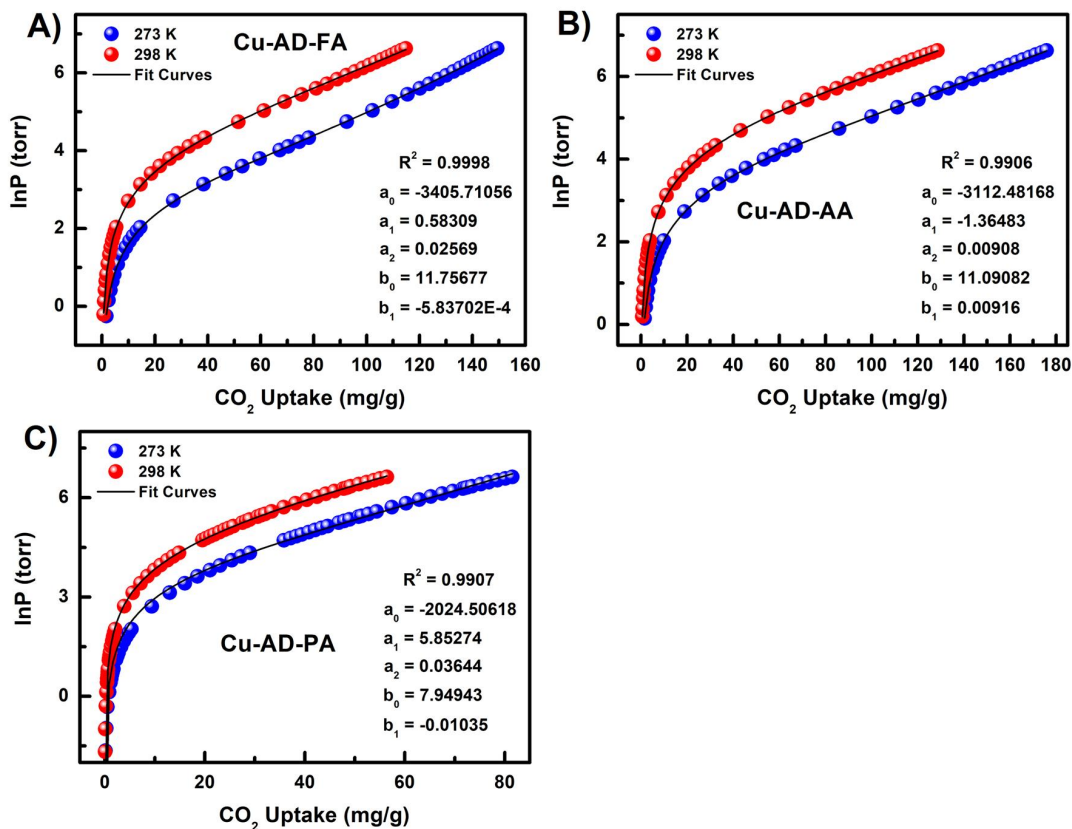
Supplementary Figure 17. Nonlinear curves fitting of CO_2 for (A) **Cu-AD-FA**, (B) **Cu-AD-AA**, (C) **Cu-AD-PA**.
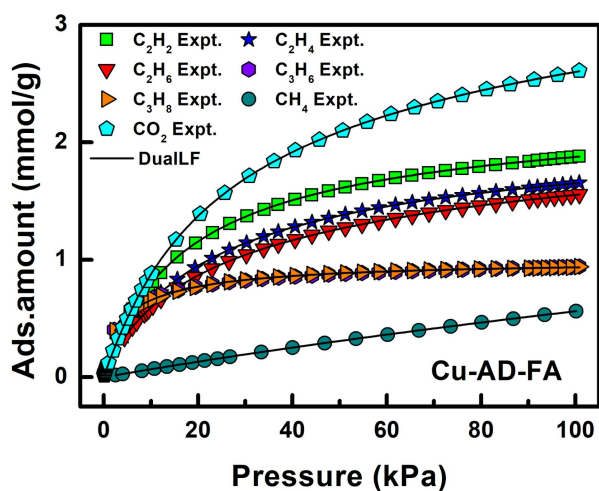
Supplementary Figure 18. Cu-AD-FA at 298 K along with the dual-site Langmuir Freundlich (DSLF) fits.
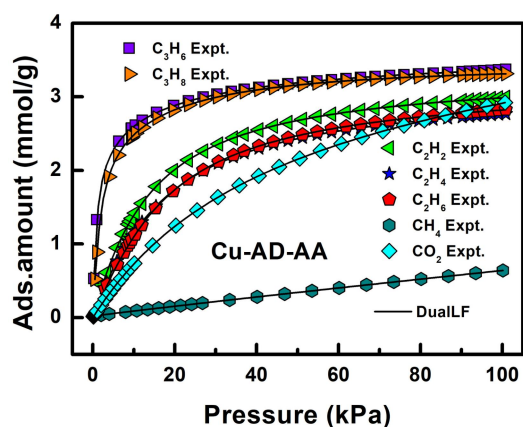
Supplementary Figure 19. Cu-AD-AA at 298 K along with the dual-site Langmuir Freundlich (DSLF) fits.
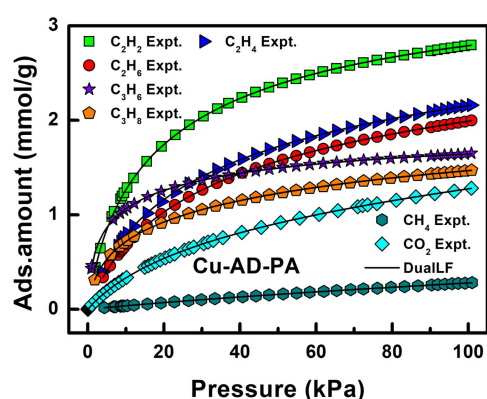
Supplementary Figure 20. Cu-AD-PA at 298 K along with the dual-site Langmuir Freundlich (DSLF) fits.
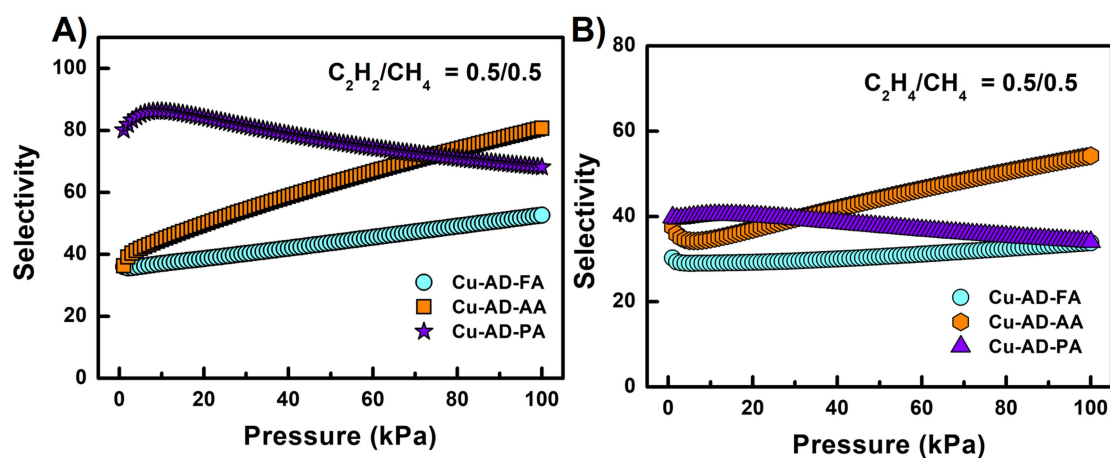
Supplementary Figure 21. Selectivity of predicted by IAST at 298 K and 101 kPa (A) C_2H_2/CH_4 (0.5/0.5), (B) C_2H_4/CH_4 (0.5/0.5).
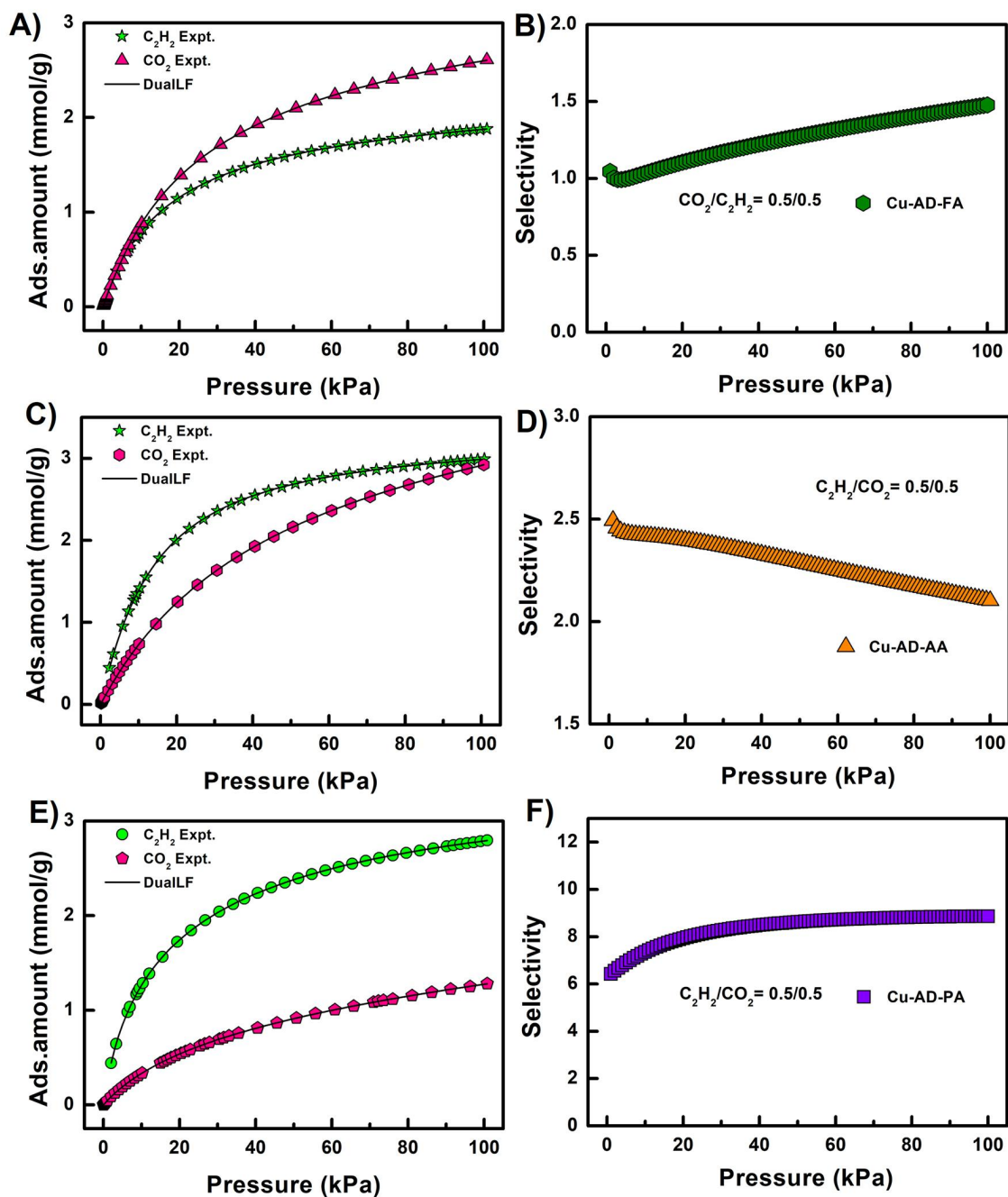
Supplementary Figure 22. C_2H_2 and CO_2 at 298 K along with the dual-site Langmuir Freundlich (DSLF) fits for (A) **Cu-AD-FA**, (C) **Cu-AD-AA**, (E) **Cu-AD-PA**. Selectivity of predicted by IAST at 298 K and 101 kPa: (B) CO_2/C_2H_2 (0.5/0.5) for **Cu-AD-FA**, (D) C_2H_2/CO_2 (0.5/0.5) for **Cu-AD-AA**, (F) C_2H_2/CO_2 (0.5/0.5) for **Cu-AD-PA**.
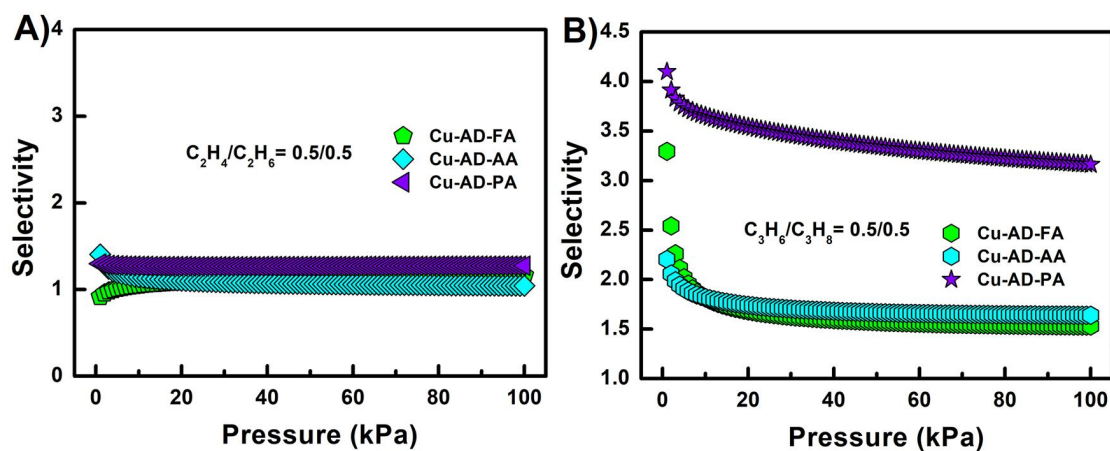
Supplementary Figure 23. Selectivity of predicted by IAST at 298 K and 101 kPa (A) C_2H_4/C_2H_6 (0.5/0.5), (B) C_3H_6/C_3H_8 (0.5/0.5).
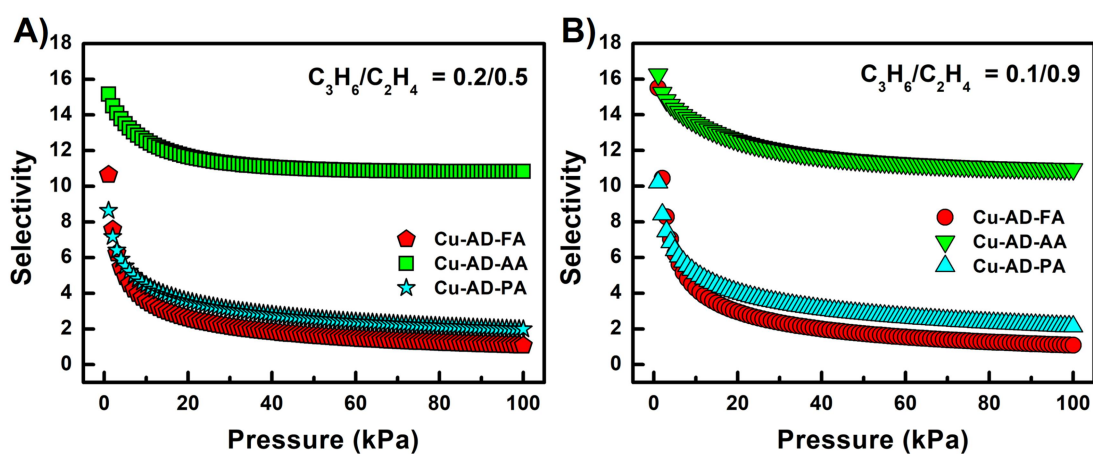
Supplementary Figure 24. Selectivity of predicted by IAST at 298 K and 101 kPa (A) C_3H_6/C_2H_4 (0.2/0.5), (B) C_3H_6/C_2H_4 (0.1/0.9).
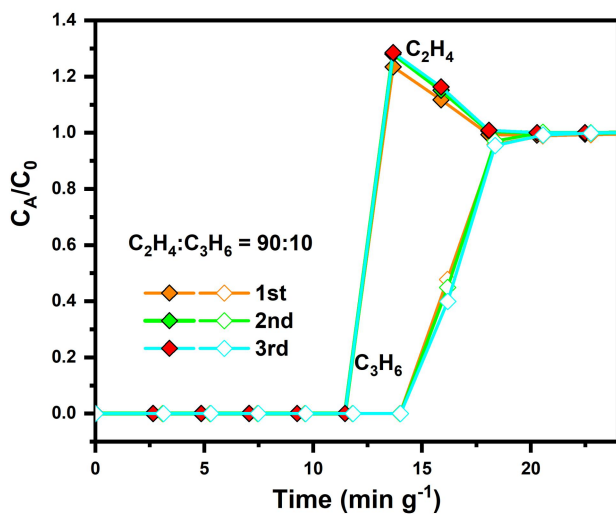
Supplementary Figure 25. The breakthrough curves of the C_2H_4/C_3H_6 mixtures (v/v = 90/10 under a flow of 5 mL/min).
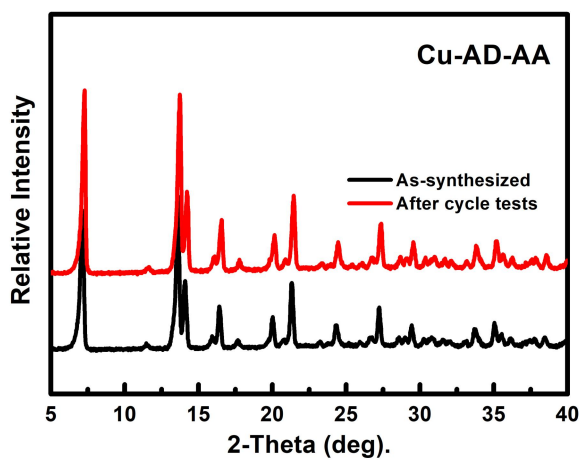
Supplementary Figure 26. PXRD patterns after breakthrough cycle tests for **Cu-AD-AA**.

Calculation procedures of selectivity from IAST

The measured experimental data are excess loadings (q^{ex}) of the pure components CH_4, C_2H_2, C_2H_4, C_2H_6, C_3H_6 and C_3H_8 for **Cu-AD-FA**, **Cu-AD-AA** and **Cu-AD-PA**, which should be converted to absolute loadings (q) firstly.

$$q = q^{ex} + \frac{pV_{pore}}{ZRT} \qquad (1)$$

Here Z is the compressibility factor. The Peng-Robinson equation (Eq. 1) is used to estimate the value of compressibility factor to obtain the absolute loading, while the measure pore volume is also necessary.

The dual-site Langmuir-Freundlich equation (Eq. 2) is used for fitting the isotherm data at 298 K.

$$q = q_{m_1} \times \frac{b_1 \times p^{1/n_1}}{1+b_1 \times p^{1/n_1}} + q_{m_2} \times \frac{b_2 \times p^{1/n_2}}{1+b_2 \times p^{1/n_2}} \qquad (2)$$

Here p is the pressure of the bulk gas at equilibrium with the adsorbed phase (kPa), q is the adsorbed amount per mass of adsorbent (mol kg^{-1}), q_{m1} and q_{m2} are the saturation capacities of sites 1 and 2 (mol kg^{-1}), b_1 and b_2 are the affinity coefficients of sites 1 and 2 (1/kPa), n_1 and n_2 are the deviations from an ideal homogeneous surface.

$$S = \frac{q_1/q_2}{p_1/p_2} \qquad (3)$$

The selectivity of preferential adsorption of component 1 over component 2 in a mixture containing 1 and 2, perhaps in the presence of other components too, can be formally defined as q_1 and q_2 are the absolute component loadings of the adsorbed phase in the mixture. These component loadings are also termed the uptake capacities. We calculate the values of q_1 and q_2 using the Ideal Adsorbed Solution Theory (IAST) of Myers and Prausnitz (Eq. 3).
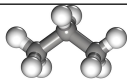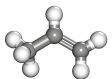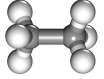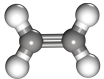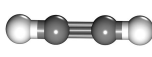
Supplementary Table 1. Crystal data and structure refinement of Cu-AD-FA

MOF	Cu-AD-FA
formula	$C_{27}H_{39}Cu_3N_{18}O_9$
formula Weight	949.04
temperature	303.0 K
wavelength	0.71073 Å
crystal system, space group	Tetragonal, $I4_1/a$
a (Å)	15.2500(2)
b (Å)	15.2500(2)
c (Å)	22.9611(4)
V (Å^3)	5339.89(17)
Z, D_c (Mg/M^3)	5.33333, 1.574
F (000)	2588.0
θ range (deg)	5.182~50.696
reflns collected/unique	8227/2420
R_{int}	0.0167
data/restraints/params	2420/12/175
GOF on F^2	1.065
R_1, wR_2 (I>2σ(I))	R_1=0.0298, wR_2=0.0861
R_1, wR_2 (all data)	R_1=0.0334, wR_2=0.0894
CCDC No.	2312625

Supplementary Table 2. Unit cell parameters of Cu-AD-FA, Cu-AD-AA, BIO-MOF-11 and BIO-MOF-12

MOF	Cu-AD-FA	Cu-AD-AA	BIO-MOF-11	BIO-MOF-12
crystal system, space group	Tetragonal, $I4_1/a$	Tetragonal, $I4_1/a$	Tetragonal, $I4_1/a$	Tetragonal, $I4_1/a$
a (Å)	15.2500(2)	15.298(1)	15.4355(18)	17.243(3)
b (Å)	15.2500(2)	15.298(1)	15.4355(18)	17.243(3)
c (Å)	22.9611(4)	22.517(3)	22.775(5)	20.157(6)
V (Å^3)	5339.89(17)	5269.6(8)	5426.3(16)	5993(2)
CCDC nmuber	2312625	817663	785771	914678

Supplementary Table 3. Physical parameters of C_1-C_3 light hydrocarbon

Gas	Structure	Molecular size (Å^3)	Kinetic diameter (Å)	Boiling point (K)	Polarizability (×10^{-25}/cm^3)	Dipole moment (10^{18}/esu cm^2)	Quadrupole moment (10^{26}/esu cm^2)
C_3H_8		4.02×4.52×6.61	4.3-5.118	231.1	62.9-63.7	0.084	
C_3H_6		4.16×4.65×6.44	4.678	225.4	62.6	0.366	
C_2H_6		4.08×3.81×4.82	4.443	184.5	44.3-44.7	0	0.65
C_2H_4		3.28×4.18×4.84	4.163	169.4	42.52	0	1.50
C_2H_2		3.32×3.34×5.70	3.3	189.3	33.3-39.3	0	7.50
CH_4		3.7×3.7×3.7	3.8	111.6	26	0	0

Supplementary Table 4. The adsorption capacity of C_1-C_3 light hydrocarbons at 10 kPa and 101 kPa and 298 K

MOFs	CH_4 (cm³/g)		C_2H_2 (cm³/g)		C_2H_4 (cm³/g)		C_2H_6 (cm³/g)		C_3H_6 (cm³/g)		C_3H_8 (cm³/g)	
	10 kPa	101 kPa	10 kPa	101 kPa	10 kPa	101 kPa	10 kPa	101 kPa	10 kPa	101 kPa	10 kPa	101 kPa
Cu-AD-FA	0.9	7	18	42	15	37	14	35	17	21	16	21
Cu-AD-AA	1.2	10	32	67	26	62	25	63	59	75	56	74
Cu-AD-PA	0.8	6	29	60	17	48	15	45	24	37	16	33

Supplementary Table 5. The refined parameters for the Dual-site Langmuir-Freundlich equations fit for the pure isotherms of CO_2, CH_4, C_2H_2, C_2H_4, C_2H_6, C_3H_6 and C_3H_8 for Cu-AD-FA at 298 K

		q_{m1}	q_{m2}	b_1	b_2	n_1	n_2	R^2
	C_3H_6	0.86666	0.25632	0.3781	0.22462	0.50167	1.17884	0.99999
Cu-AD-FA	CH_4	1.13224	0.15907	6.29254E-4	0.01755	1.25519	1.0222	0.99999
	C_2H_6	1.26222	1.15771	0.0723	0.01565	0.92691	0.83985	0.99999
	C_3H_8	0.39279	0.60048	1.00048	0.08155	1.33034	1.03194	0.99998
	C_2H_2	2.06556	1.58491	0.06223	0.00163	0.98702	0.83342	0.99999
	C_2H_4	1.77917	0.36469	0.03968	0.10057	0.92325	1.07521	0.99999
	CO_2	1.53498	2.88142	0.03444	0.02391	1.19298	0.74631	0.99999

Supplementary Table 6. The refined parameters for the Dual-site Langmuir-Freundlich equations fit for the pure isotherms of CO_2, CH_4, C_2H_2, C_2H_4, C_2H_6, C_3H_6 and C_3H_8 for Cu-AD-AA at 298 K

		q_{m1}	q_{m2}	b_1	b_2	n_1	n_2	R^2
Cu-AD-AA	C_3H_6	2.60968	1.14829	0.29544	1.79465	0.63973	1.5056	0.99999
	CH_4	9.662E-4	2.08571	4.14389E6	0.00245	0.98579	1.00695	0.99999
	C_2H_6	2.34214	0.93952	0.05842	0.00932	0.94495	1.70868	0.99999
	C_3H_8	1.07752	2.38268	0.0288	0.5823	1.19812	1.19361	0.99999
	C_2H_2	2.29709	1.06541	0.08159	0.02857	0.94585	1.37165	0.99999
	C_2H_4	2.30857	0.91897	0.03117	0.11119	1.24991	0.68962	0.99999
	CO_2	3.98438	1.92179	0.02212	3.86292E-5	1.00144	1.69156	0.99999

Supplementary Table 7. The refined parameters for the Dual-site Langmuir-Freundlich equations fit for the pure isotherms of CO_2, CH_4, C_2H_2, C_2H_4, C_2H_6, C_3H_6 and C_3H_8 for Cu-AD-PA at 298 K

		q_{m1}	q_{m2}	b_1	b_2	n_1	n_2	R^2
Cu-AD-PA	C_3H_6	1.24681	0.71553	0.50149	0.04201	0.71368	0.84736	0.99998
	CH_4	0.09586	5.33509	0.00911	6.27503E-4	1.09597	0.92081	0.99997
	C_2H_6	1.89565	2.77283	0.05141	0.00391	0.95344	0.85502	0.99999
	C_3H_8	0.74747	1.50165	0.30644	0.02544	0.83331	0.80806	0.99999
	C_2H_2	2.47706	1.11531	0.04001	0.15737	0.8856	1.00091	0.99999
	C_2H_4	2.24275	0.78332	0.06093	5.72062E-4	0.93237	1.54409	0.99999
	CO_2	0.66199	3.65487	0.04231	0.00522	1.02715	0.83886	0.99999

Supplementary Table 8. Comparison of the selectivity for C$_3$H$_8$/CH$_4$ (v/v = 0.5/0.5) and C$_2$H$_6$/CH$_4$ (v/v = 0.5/0.5) with other reported materials at 298 K under 101 kPa

MOFs	C$_3$H$_8$ (cm^3/g)	C$_2$H$_6$ (cm^3/g)	CH$_4$ (cm^3/g)	C$_3$H$_8$/CH$_4$	C$_2$H$_6$/CH$_4$	Ref.
BSF-2	39.6	27.3	5.4	2609	53	[1]
Ni(HBTC)(bipy)	138.4	131.0	20.8	1857.0	27.5	[2]
MIL-142A	119.2	85.6	12.1	1300	13.7	[3]
JUC-220				873	39	[4]
JLU-Liu40	164	104	11	845	21	[5]
Cu-IPA	69.4	57.6	18.1	765	40	[6]
UiO-66-Naph	31.1	27.8	8.5	741	32	[7]
ZUL-C2	56.5	63.2		632	91	[8]
JLU-MOF68	95.0		6.2	628		[9]
PCN-224	184.8	65.9	10.5	609	12	[10]
FJI-C1	141.9	87.4	9.7	471		[11]
BSF-1	43.5	35.2	10.5	353	23	[12]
NKM-101a	74.9	65.5	15.1	223.1	20.1	[13]
UPC-100-In	118.9	119.3	11.7	186.4	26.6	[14]
CTGU-15	271.7	47.7	8.96	170.7	5.2	[15]
Cu-AD-FA	21	35	7	29.1	36.6	This work
Cu-AD-AA	74	63	10	746.1	50.0	This work
Cu-AD-PA	33	45	6	31.1	27.8	This work

Supplementary Table 9. Comparison of the selectivity for C_3H_6/C_2H_4 with other reported materials at 298 K under 101 kPa

MOFs	C_3H_6 (cm³/g)	C_2H_4 (cm³/g)	IAST 0.5/0.5	0.2/0.5	0.1/0.9	Ref.
Zn₂(oba)₂(dmimpym)	76.0	48.3	15.6	16.5	17.1	[16]
CoV-(CF₃)₃bdc-tpt	79.1	65.9	10.1			[17]
CoIn-bco-tpt	98.8	90.9	9.14			[17]
CoV-bco-tpt	109.9	102.8	7.83			[17]
CoIn-bco-tpa	81.1	67.8	6.10			[17]
CoV-bco-tpa	76.4	64.9	6.37			[17]
Y-pek-MOF-1	146.3	47.2	9.0			[18]
Y-pek-MOF-2	127.3	41.7	5.4			[18]
NEM-7-Cu	75.5	29	8.61			[19]
Mn-dtzip	216.4	76.7	8.6	8.7	9.0	[20]
spe-MOF	236.9	48.9	7.7	7.0	6.7	[21]
srl-MOF	30.1	21.4	8.09			[21]
MFM-202a	160.8	64.9	8.4			[22]
Iso-MOF-1	209.0	51.0	5.08		5.36	[23]
Iso-MOF-2	254.1	71.4	6.60		6.81	[23]
Iso-MOF-3	234.7	66.0	7.04		7.12	[23]
Iso-MOF-4	254.5	73.1	7.74		7.23	[23]
UPC-33	94.3	31.1	5.70		5.84	[24]
Zn-BPZ-SA	68.3	63.9	4.8	5.3	6.1	[25]
Mg-MOF-74			4.7			[26]
Ni-MOF-74			3.3			[26]
Cd₂(AzDC)₂(TPT)₂](DMF)₃	59.84	44.95	1.2			[27]
Cu-AD-FA	21	37	1.1	1.1	1.1	This work
Cu-AD-AA	75	62	10.9	10.8	10.9	This work
Cu-AD-PA	37	48	1.9	2.0	2.1	This work

REFERENCES

1.   Zhang Y, Yang L, Wang L, Cui X, Xing H. Pillar iodination in functional boron cage hybrid supramolecular frameworks for high performance separation of light hydrocarbons. *J Mater Chem A* 2019;7:27560-66. DOI: 10.1039/c9ta09928j

2.   Guo P, Chang M, Yan T, Li Y, Liu D. A pillared-layer metal–organic framework for efficient separation of $C_3H_8/C_2H_6/CH_4$ in natural gas. *Chin J Chem Eng* 2022;42:10-16. DOI: 10.1016/j.cjche.2021.08.011

3.   Yuan Y, Wu H, Xu Y, et al. Selective extraction of methane from C1/C2/C3 on moisture-resistant MIL-142A with interpenetrated networks. *Chem Eng J* 2020;395:125057. DOI: 10.1016/j.cej.2020.125057

4.   Shi X, Zu Y, Li X, et al. Highly selective adsorption of light hydrocarbons in a HKUST-like MOF constructed from spirobifluorene-based octacarboxylate ligand by a substitution strategy. *Nano Research* 2023;16:10652-59. DOI: 10.1007/s12274-023-5634-x

5.   Sun Q, Yao S, Liu B, et al. A novel polyhedron-based metal-organic framework with high performance for gas uptake and light hydrocarbon separation. *Dalton Trans* 2018;47:5005-10. DOI: 10.1039/C7DT04622G

6.   Lin D, Tu S, Yu L, et al. Highly efficient separation of $CH_4/C_2H_6/C_3H_8$ from natural gas on a novel copper-based metal–organic framework. *Ind Eng Chem Res* 2023;62:5252-61. DOI: 10.1021/acs.iecr.2c04286

7.   Zhang L, Xiong XH, Meng LL, et al. Engineering pore nanospaces by introducing aromatic effects in UiO-66 for efficient separation of light hydrocarbons. *J Mater Chem A* 2023;11:12902-09. DOI: 10.1039/d2ta09338c

8.   Zhou J, Ke T, Steinke F, et al. Tunable confined aliphatic pore environment in robust metal-organic frameworks for efficient separation of gases with a similar structure. *J Am Chem Soc* 2022;144:14322-29. DOI: 10.1021/jacs.2c05448

9.   Kan L, Luo X, Yu X, Zhang L, Liu Y. A multi-functionalized MOF with unique molecular-sized pockets for excellent lead(II) removal and selective separation of C_3H_8/CH_4. *Sep Purif Technol* 2023;325:124758. DOI: 10.1016/j.seppur.2023.124758

10. Shi R, Lv D, Chen Y, et al. Highly selective adsorption separation of light hydrocarbons with a porphyrinic zirconium metal-organic framework PCN-224. *Sep Purif Technol* 2018;207:262-68. DOI: 10.1016/j.seppur.2018.06.064

11. Huang Y, Lin Z, Fu H, et al. Porous anionic indium-organic framework with enhanced gas and vapor adsorption and separation ability. *ChemSusChem*

2014;7:2647-53. DOI: 10.1002/cssc.201402206

12. Zhang Y, Yang L, Wang L, Duttwyler S, Xing H. A microporous metal-organic framework supramolecularly assembled from a Cu(II) dodecaborate cluster complex for selective gas separation. *Angew Chem Int Ed Engl* 2019;58:8145-50. DOI: 10.1002/anie.201903600

13. Qiao Y, Chang X, Zheng J, et al. Self-interpenetrated water-stable microporous metal-organic framework toward storage and purification of light hydrocarbons. *Inorg Chem* 2021;60:2749-55. DOI: 10.1021/acs.inorgchem.0c03618

14. Fan W, Wang X, Xu B, et al. Amino-functionalized MOFs with high physicochemical stability for efficient gas storage/separation, dye adsorption and catalytic performance. *J Mater Chem A* 2018;6:24486-95. DOI: 10.1039/c8ta07839d

15. Lv D, Liu Z, Xu F, et al. A Ni-based metal-organic framework with super-high C_3H_8 uptake for adsorptive separation of light alkanes. *Sep Purif Technol* 2021;266:118198. DOI: 10.1016/j.seppur.2020.118198

16. Li YZ, Wang GD, Krishna R, et al. A separation MOF with O/N active sites in nonpolar pore for one-step C_2H_4 purification from C_2H_6 or C_3H_6 mixtures. *Chem Eng J* 2023;466:143056. DOI: 10.1016/j.cej.2023.143056

17. Xiao Y, Hong A N, Chen Y, et al. Developing water-stable pore-partitioned metal-organic frameworks with multi-level symmetry for high-performance sorption applications. *Small* 2023;19:e2205119. DOI: 10.1002/smll.202205119

18. Wei WQ, Guo XA, Zhang ZH, Zhang YF, Xue DX. Topology-guided synthesis and construction of amide-functionalized rare-earth metal–organic frameworks. *Inorg Chem Commun* 2021;133:108896. DOI: 10.1016/j.inoche.2021.108896

19. Liu X, Hao C, Li J, et al. An anionic metal–organic framework: metathesis of zinc(II) with copper(II) for efficient C_3/C_2 hydrocarbon and organic dye separation. *Inorg Chem Front* 2018;5:2898-905. DOI: 10.1039/c8qi00773j

20. Zhang L, Ma LN, Wang GD. et al. A new honeycomb MOF for C_2H_4 purification and C_3H_6 enrichment by separating methanol to olefin products. *J Mater Chem A* 2023;11:2343-48. DOI: 10.1039/d2ta08977g

21. Fang H, Zheng B, Zhang ZH, et al. Ligand-conformer-induced formation of zirconium-organic framework for methane storage and MTO product separation. *Angew Chem Int Ed Engl* 2021;60:16521-28. DOI: 10.1002/anie.202103525

22. Gao S, Morris CG, Lu Z, et al. Selective hysteretic sorption of light hydrocarbons

in a flexible metal–organic framework material. *Chem Mater* 2016;28:2331-40. DOI: 10.1021/acs.chemmater.6b00443

23. Fan W, Wang X, Zhang X, et al. Fine-tuning the pore environment of the microporous Cu-MOF for high propylene storage and efficient separation of light hydrocarbons. *ACS Cent Sci* 2019;5:1261-68. DOI: 10.1021/acscentsci.9b00423

24. Fan W, Wang Y, Zhang Q, et al. An amino-functionalized metal-organic framework, based on a rare $Ba_{12}(COO)_{18}(NO_3)_2$ cluster, for efficient $C_3/C_2/C_1$ separation and preferential catalytic performance. *Chem Eur J* 2018;24:2137-43. DOI: 10.1002/chem.201704629

25. Wang GD, Krishna R, Li YZ, et al. Rational construction of ultrahigh thermal stable MOF for efficient separation of MTO products and natural gas. *ACS Mater Lett* 2023;5:1091-99. DOI: 10.1021/acsmaterialslett.3c00096

26. Wu X, Bao Z, Yuan B, et al. Microwave synthesis and characterization of MOF-74 (M = Ni, Mg) for gas separation. *Microporous Mesoporous Mater* 2013;180:114-22. DOI: 10.1016/j.micromeso.2013.06.023

27. Zhang Y, Meng XQ, Ding HJ, et al. Rational construction of breathing metal-organic frameworks through synergy of a stretchy ligand and highly variable π-π interaction. *ACS Appl Mater Interfaces* 2019;11:20995-1003. DOI: 10.1021/acsami.9b04759